# Supplementary Information

## Limb development genes underlie variation in human fingerprint patterns

Jinxi Li,[1,2,27] James D. Glover,[3,27] Haiguo Zhang,[4,27] Meifang Peng,[2,4,27] Jingze Tan,[4] Chandana Basu Mallick,[3,5] Dan Hou,[6] Yajun Yang,[4] Sijie Wu,[2] Yu Liu,[2] Qianqian Peng,[2] Shijie Zheng,[2] Edie I. Crosse, [7] Alexander Medvinsky, [7] Richard A. Anderson, [8] Helen Brown,[3] Ziyu Yuan, [9] Shen Zhou[10], Yanqing Xu[11], John P. Kemp,[12] Yvonne Y.W. Ho,[13] Danuta Z. Loesch,[14] Lizhong Wang,[15] Yingxiang Li,[15] Senwei Tang,[15] Xiaoli Wu,[15] Robin G. Walters,[16] Kuang Lin,[16] Ruogu Meng,[17] Jun Lv,[18] Jonathan M. Chernus,[19] Katherine Neiswanger,[20] Eleanor Feingold,[19] David M. Evans,[12] Sarah E. Medland,[13] Nicholas G. Martin,[13] Seth M. Weinberg,[19,20,21] Mary L. Marazita,[19,20,22,23] Gang Chen,[15] Zhengming Chen,[16] Yong Zhou,[24] Michael Cheeseman,[3] Lan Wang,[6] Li Jin,[1,2,25,28,*] Denis J. Headon,[3,28,*] Sijia Wang[2,26,28,29*]

### Supplementary Text

### Transverse digital ridges as a murine model of human dermatoglyphs

We examined the structures on the ventral side of the mature mouse forepaw to assess candidate structures for modelling the human dermatoglyph ridges. Chemical removal of the epidermis followed by staining with toluidine blue reveals the arrangement of the uppermost dermal structures. In mouse this approach leads to visualization of different types of dermal structures in the forepaw (Tsugane and Yasuda, 1995). The contact surface of the foot sole has large pads, which have been termed cobblestone, interdigital, or carpal pads. The digits themselves have a series of transverse parallel ridges, some complete, some interrupted and some partial. The digit tips have a single pad with very fine reticulated network of dermal ridges under the epidermis (Tsugane and Yasuda, 1995), which differs from the other dermal structures detected in that they are not present in the topology of the skin surface, which is smooth. This provides a range of candidate structures for comparison to human dermatoglyph ridges.

As human fingerprint patterns are established before birth, we explored the developmental origin of dermatoglyphs in mouse embryos. We found that the transverse digit ridges are apparent prior to birth, at embryonic day 17.5 (E17.5), as a set of stripes visualized in the WNT reporter TCF/LEF::H2B-GFP line (Ferrer-Vaquer et al., 2010) (Figure S2A). Thus the ridge patterns in

mouse digits emerge prenatally and prior to physical functioning of the digits, as do the dermatoglyph ridges in human. Newborn pups at postnatal day 1 (P1) already have both continuous and discontinuous ridges, which become more distinct by toluidine blue staining in the subsequent stages (Figure S2B).

In humans, a profound distortion of dermatoglyph pattern is a characteristic of the condition hypohidrotic ectodermal dysplasia, such that ridges are reduced and distorted, with fingerprint patterns sometimes indecipherable (Kargul et al., 2001; Verbov, 1970). This condition is caused by mutations in the *EDA*, *EDAR* or *EDARADD* genes, and also causes reduction or absence of hairs, teeth and a number of types of glands. We investigated dermal structures on the forelimb of $Eda^{Tabby}$ and $Edar^{downless.J}$ mutant mice, these being models of human hypohidrotic ectodermal dysplasia (Headon and Overbeek, 1999; Kowalczyk-Quintas and Schneider, 2014; Monreal et al., 1999; Srivastava et al., 1997). The cobblestone pads of the palmar surface and the fine patterns at the digit tips were not notably altered in these mutants when compared to control mice, but the transverse digital ridges were markedly distorted and diminished (Figures S2C). This supports the transverse digital ridges as the closest identifiable homologs of human dermatoglyphs, due to their shared and selective requirement for EDA function for their normal development.

Based on their location on ventral side of digits, prenatal formation, parallel periodic arrangement transverse to the long axis of the digit, presence of Merkel cells from early in development (data not shown), carrying of eccrine sweat gland pores, and selective disruption of their pattern by EDA or EDAR pathway mutations, we conclude that transverse digital ridges in mouse serve as the best model of human dermatoglyphs. These transverse ridges in mouse cover only approximately the proximal two-thirds of the digit, with the distal portion having a smooth surface. Thus these transverse ridges are akin to the ridges running across the proximal two phalanges on the human digit, rather than the more complex patterns of the human digit tip.

## Supplemental Methods

## Supplemental Figures

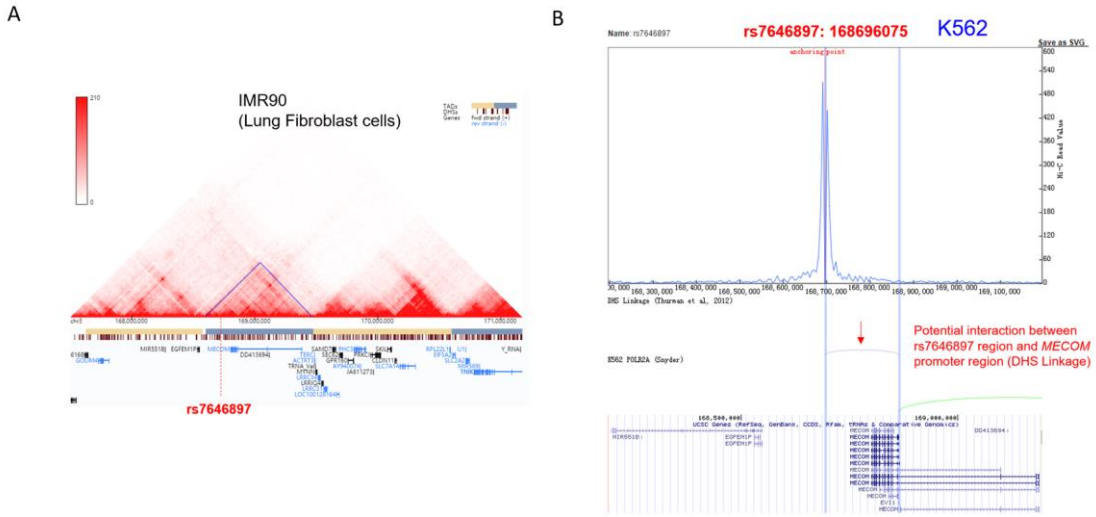


**Figure S1. Visualizing chromatin interaction between the *EVI1* gene, enhancer and the rs7646897 region.**

(A) Visualization of genome structure by Hi-C data as a heatmap indicated that the rs7646897 region and *EVI1* are located within the same TAD surveyed in 3D genome browser.

(B) Combined with three methods implemented in 3D Genome browser: Virtual 4C (Circular chromosomal conformation capture, top) that surveys for one-vs-many interactions in the genome, DNase I Hypersensitivity Site linkage (middle) that detects distal-proximal DHSs pairs, and ChIA-PET (bottom) that detects long-range interactions between genomic regions, chromatin interactions were identified between promoter region of the *EVI1* gene and enhancer harboring SNP rs7646897 (primarily supported by the DHS-linkage data).

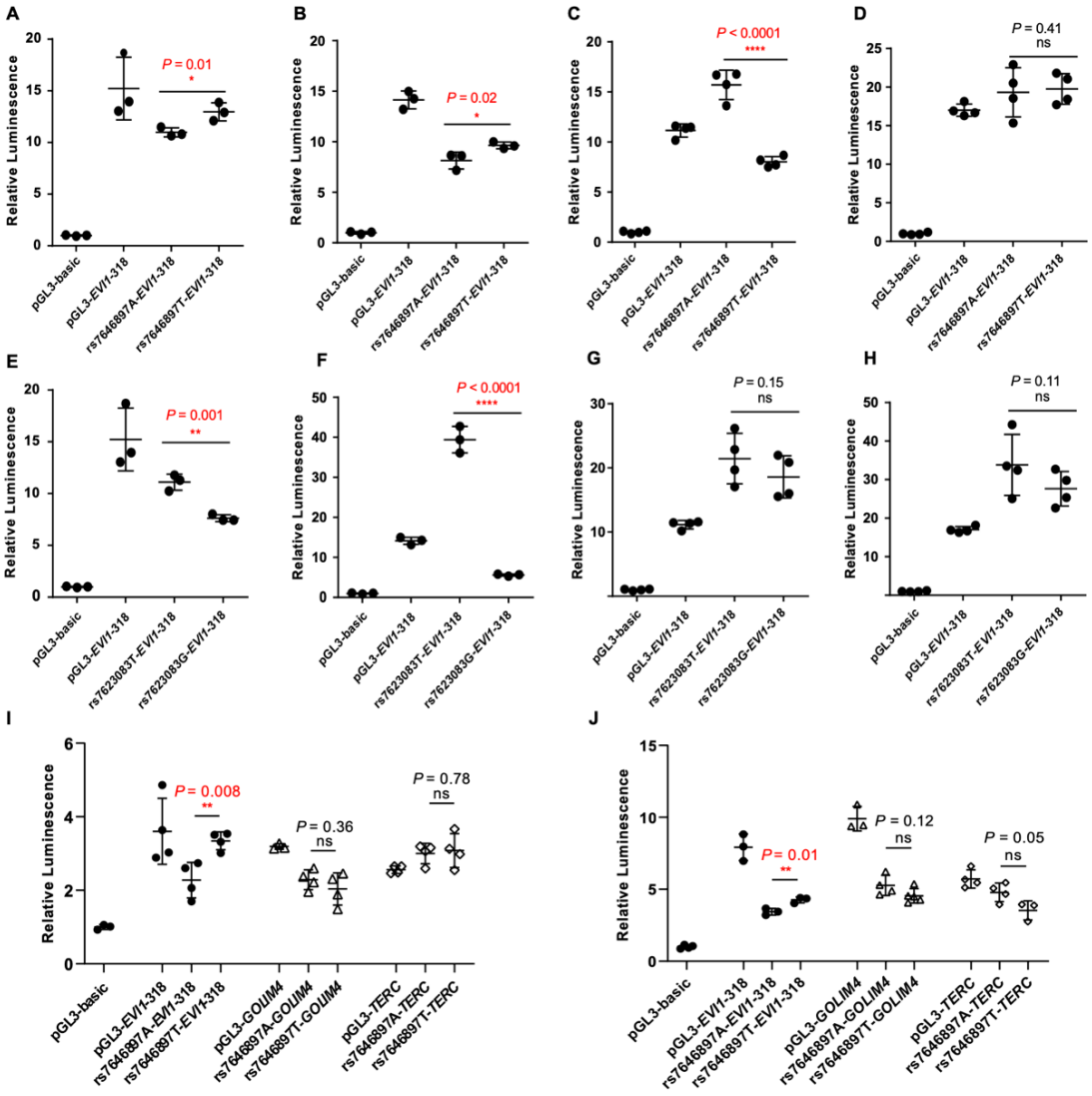


**Figure S2. Independent luciferase reporter assays on candidate regulatory elements carrying alternate alleles at SNPs rs7646897 in HEK293T cells.**

(A-D) Four independent luciferase reporter assays to test the changes of rs7646897 modulating the expression of *EVI1*. Three out of four experiments confirmed the regulatory activity.

(E-H) Four independent luciferase reporter assays to test the changes of rs7623083 modulating the expression of *EVI1*. The effect of rs7623083 on modulating expression of *EVI1* is inconsistent.

(I-J) Two independent luciferase reporter assays to test whether SNP rs7646897 modulates the expression of other closest up- and downstream genes *GOLIM4* and *TERC*.

pGL3-basic is a negative control plasmid lacking enhancer activity, pGL3-EVI1, pGL3-GOLIM4 and pGL3-TERC are the positive controls derived from EVI1, GOLIM4 and TERC promoter region, respectively. Symbols indicate significance in t test (*P<0.05, **<0.01, ***<0.001).

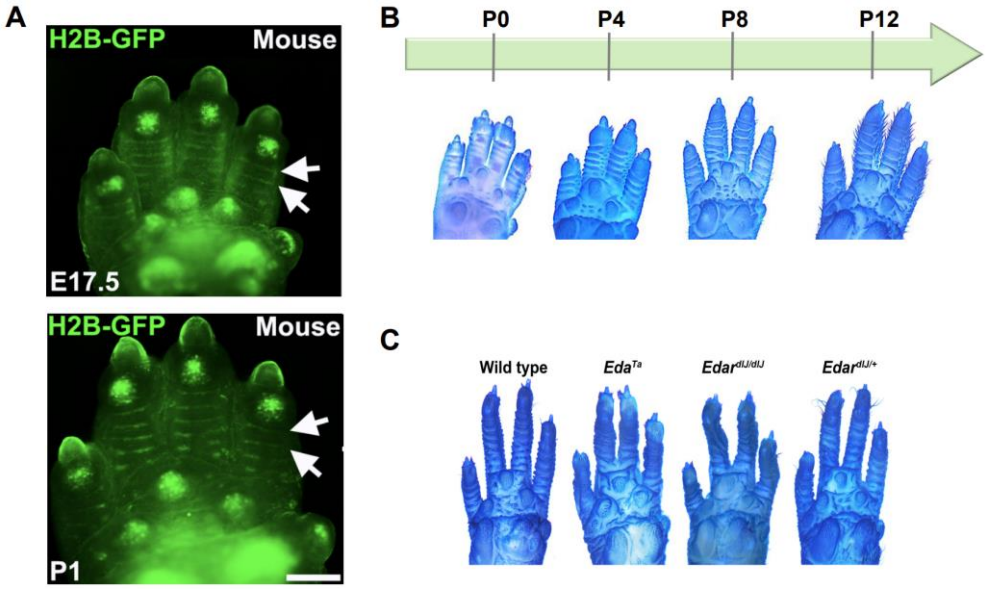


**Figure S3. Development of digit ridge pattern in mouse.** A) Embryonic origin of digit ridge pattern in mouse. Ventral views of forelimbs of mice carrying a TCF/Lef::H2B-GFP WNT pathway reporter gene at embryonic day 17.5 (E17.5) and newborn (P1). Transverse digital ridges (examples indicated by arrows) are apparent from E17.5. Scale bar = 500 µm. B) Development of mouse digital ridge patterning through different time points starting from P0 (at birth) followed by post natal days P4, P8 and P12. C) Altered digit ridge patterns in *EDA* pathway mutant mice. Palmar dermal surface of toluidine blue stained right forepaws from wild type, $Eda^{Ta}$, $Edar^{dlJ/dlJ}$ and heterozygous $Edar^{dlJ/+}$ mice at postnatal day 21, showing footpad and digit pad types and the distorted ridge pattern in the mutants.

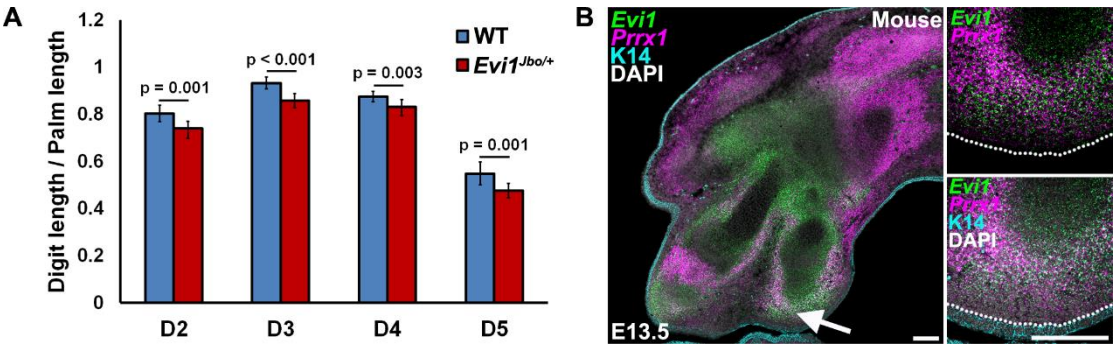


**Figure S4. *Evi1*$^{Jbo}$ effect on digit proportions and coexpression with *Prrx1*.** A) Digit length, normalized to palm length, in wild type (WT) and $Evi1^{Jbo/+}$ heterozygous adult mice. Digits are shorter in mutant animals. B) RNAscope *in situ* hybridization detecting *Evi1* and the limb mesenchyme marker *Prrx1* transcripts in mouse E13.5 embryonic limb, sectioned perpendicular to the dorsal-ventral axis. Right panels are higher magnification views of area indicated by the arrow on the left panel. Dotted line demarcates epithelium, as defined by immunofluorescent detection of KERATIN14 (K14). *Evi1* and *Prrx1* are coexpressed in mesenchymal cells, with *Evi1* also

expressed in prominently in mesenchymal cells condensing to form cartilage of the digits, as in human limb development. No expression is detected in epithelium. Nuclei are counterstained with DAPI. Scale bar = 100 μm.

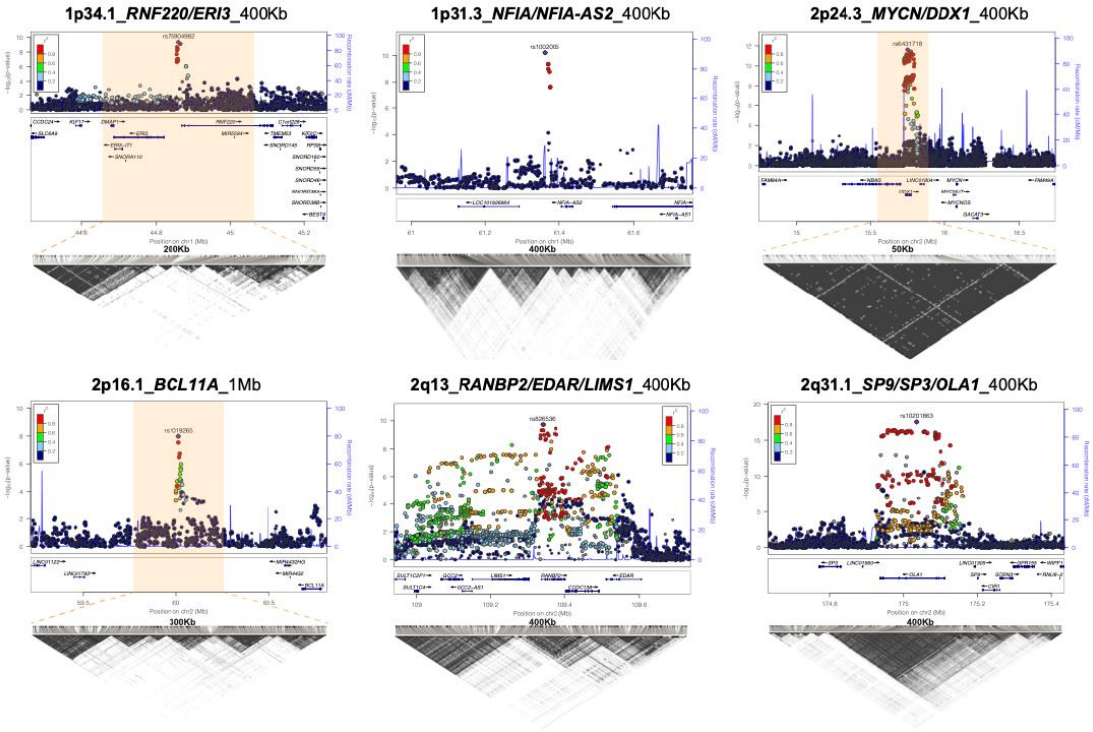


**Figure S5 Regional plots of 43 loci associated with fingerprint patterns observed in the meta-analysis across all eight cohorts.** Regional association and linkage disequilibrium plot are shown for each locus around the lead SNP (purple diamond) and the color of the remaining markers reflects the linkage disequilibrium ($r^2$) with the lead SNP. The recombination rate (right-side y axis) is plotted in blue and is based on the ASN 1000 genome population for Han Chinese. Vertical bars on the bottom represent the exons for each gene available from the hg19 UCSC Genome Brower.

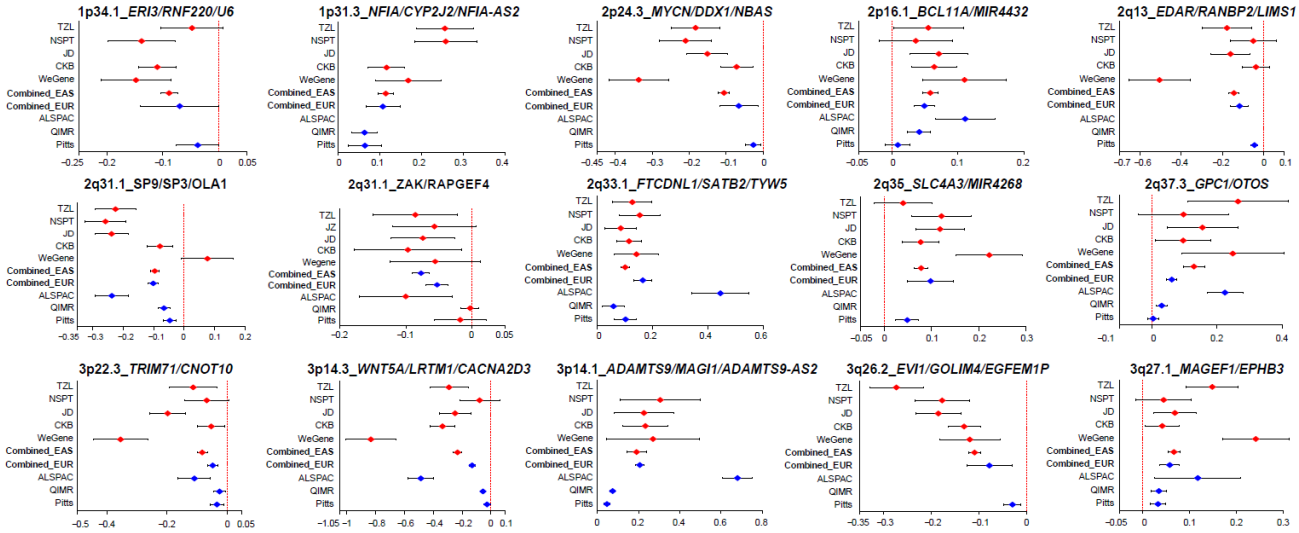


**Figure S6. Effect sizes (regression coefficients) for the derived allele at index SNPs in the genome regions associated with fingerprint patterns.** Estimates obtained in each cohort are shown as blue boxes. Box size is proportional to allele frequency of Allele1. Horizontal bars indicate confidence intervals representing 2×standard errors. Intervals that include zero (that is, non-significant effects) intersect the dashed vertical line. The estimates obtained in the Asian cohorts are shown in red boxes and those obtained in the European cohorts in blue boxes. Diamonds represent the beta and the error bars indicate the 95% confidence interval.

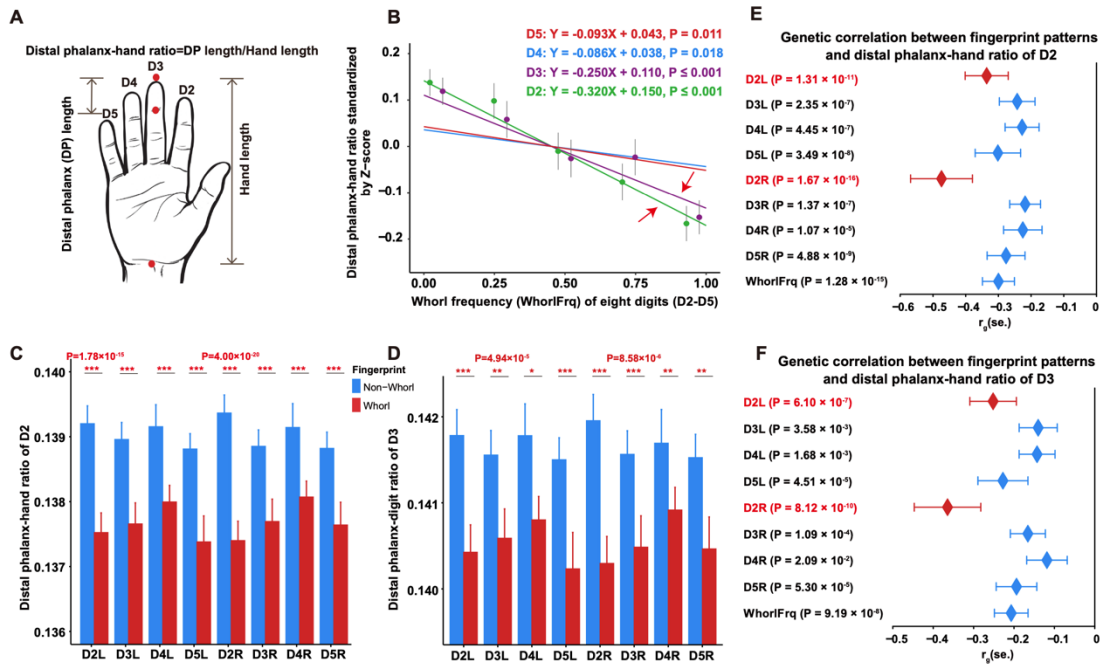


**Figure S7. Association between fingerprint patterns and hand proportions.** A) Diagrammed human hand with measured phenotypes, including hand and distal phalanx length. The distal phalanx-hand ratio (DPHR) is the ratio of distal phalanx length to hand length. B) The association between the whorl frequency on eight digits and the DPHR of each digit. We used Z-score to standardize the mean DPHR of left and right hands. Solid dots indicated the average values and short black lines were standard deviation for each group. The arrow indicates the linear regression passes the significance test. C-D) Bar plot of fingerprint pattern type (non-whorl versus whorl) of each digit (D2-D5) and the mean DPHR of D2 or D3. Error bars indicate S.E.M. * $P$<0.05, ** <0.01, *** <0.001; E-F) Genetic correlations between fingerprint patterns and the mean DPHR of D2 or D3. Estimates and tests were performed using the bivariate GREML of GCTA software. Error bars indicate S.E.M.

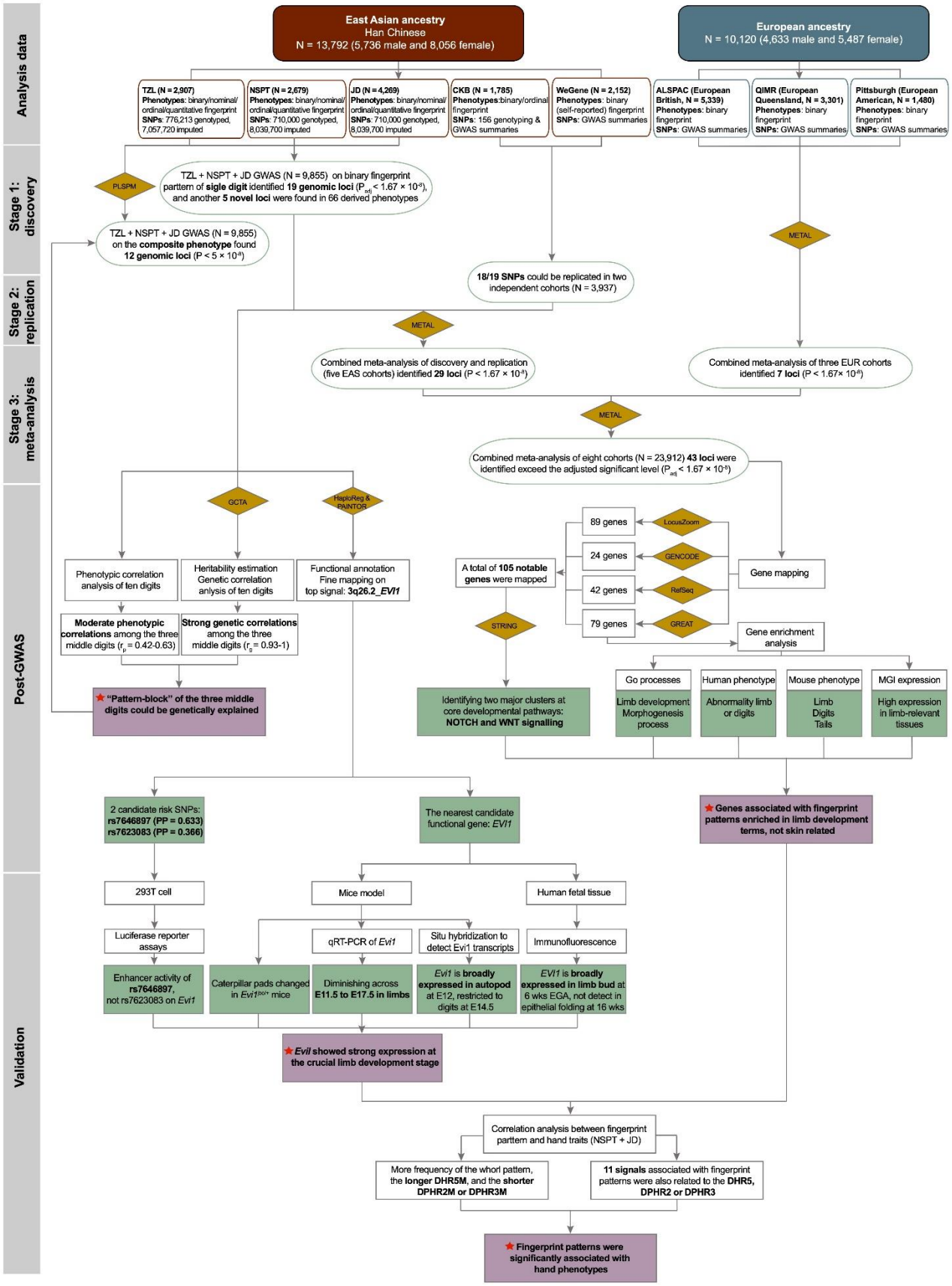


**Figure S8. Flow chart of analyses conducted in the study of fingerprint patterns.** Flowchart depicting strategy for the association analysis and functional validation, as well as numbers of

samples and SNPs by stage. The yellow diamonds represent bioinformatics tools and software, the green box indicates the main results of the analysis, and the purple box (asterisk) summarizes the conclusions of this study. Abbreviation: TZL = cohort from Taizhou Longitudinal Study, NSPT = cohort from National Survey of Physical Traits Project, JD = cohort from Jidong of Hebei Province, CKB = cohort from China Kadorie Biobank, WeGene = cohort from WeGene company, ALSPAC = The Avon Longitudinal Study of Parents and Children cohort, QIMR = The Queensland Institute of Medical Research cohort.

## Supplemental Tables

**Table S1. Characteristics of cohorts and summary of imputation methods and quality control filters**

**Table S2. Performance of signals in Han Chinese discovery and replication populations based on ordinal and binary fingerprint patterns**

**Table S3. Association results of the composite phenotype (extracted from the middle three digits of both hands)**

**Table S4. The 66 additional phenotypes derived from fingerprint patterns used in this study**

**Table S5. Transverse digit pad patterning in *Evi1*$^{Jbo}$ mice**

**Table S6. The performance of 43 signals after meta-analysis of eight populations (the top SNP in each locus was displayed)**

**Table S7. Single-factor regression analysis between hand traits and whorl frequency of eight digits (except the thumbs) in the Chinese Han populations (N=6,318, JD + NSPT)**

**Table S8. Genetic correlation (rg) based on SNP between fingerprint and hand traits in the Chinese Han populations (N=6,318, JD + NSPT)**

Ferrer-Vaquer, A., Piliszek, A., Tian, G., Aho, R.J., Dufort, D., and Hadjantonakis, A.K. (2010). A sensitive and bright single-cell resolution live imaging reporter of Wnt/ss-catenin signaling in the mouse. BMC Dev Biol *10*, 121.
Headon, D.J., and Overbeek, P.A. (1999). Involvement of a novel Tnf receptor homologue in hair follicle induction. Nat Genet *22*, 370-374.
Kargul, B., Alcan, T., Kabalay, U., and Atasu, M. (2001). Hypohidrotic ectodermal dysplasia: dental, clinical, genetic and dermatoglyphic findings of three cases. J Clin Pediatr Dent *26*, 5-12.
Kowalczyk-Quintas, C., and Schneider, P. (2014). Ectodysplasin A (EDA) - EDA receptor signalling and its pharmacological modulation. Cytokine Growth Factor Rev *25*, 195-203.
Monreal, A.W., Ferguson, B.M., Headon, D.J., Street, S.L., Overbeek, P.A., and Zonana, J. (1999). Mutations in the human homologue of mouse dl cause autosomal recessive and dominant hypohidrotic ectodermal dysplasia. Nat Genet *22*, 366-369.
Srivastava, A.K., Pispa, J., Hartung, A.J., Du, Y., Ezer, S., Jenks, T., Shimada, T., Pekkanen, M., Mikkola, M.L., Ko, M.S*., et al.* (1997). The Tabby phenotype is caused by mutation in a mouse homologue of the EDA gene that reveals novel mouse and human exons and encodes a protein (ectodysplasin-A) with collagenous domains. Proc Natl Acad Sci U S A *94*, 13069-13074.
Tsugane, M., and Yasuda, M. (1995). Dermatoglyphics on volar skin of mice: the normal pattern. The Anatomical Record *242*, 225-232.
Verbov, J. (1970). Hypohidrotic (or anhidrotic) ectodermal dysplasia--an appraisal of diagnostic methods. Br J Dermatol *83*, 341-348.